

Shape-Controlled Electrodeposition of Gold Nanostructures

Yang Tian,^{*,†} Haiqing Liu,[†] Guohua Zhao,[†] and Tetsu Tatsuma[‡]

Department of Chemistry, Tongji University, Siping Road 1239, Shanghai 200092, People's Republic of China, and Institute of Industrial Science, The University of Tokyo, 4-6-1 Komaba, Meguro-ku, Tokyo 153-8505, Japan

Received: August 16, 2006; In Final Form: September 21, 2006

A one-step, nontemplated, low-cost electrochemical method for the growth of gold nanostructures with different shapes is reported here. It is the first time that nanopyramidal, nanorod-like, and spherical gold nanostructures were fabricated on polycrystalline gold substrates through electrochemical overpotential deposition (OPD) by easily manipulating the deposited potentials and concentrations of HAuCl₄. X-ray diffraction and electrochemical analyses revealed that the pyramidal structures are more extensively dominated by (111) facets in comparison with the other nanostructures. The nanopyramids, which have anisotropic structures, exhibited broad extinction over the visible region, most likely due to plasmon resonance. Oxygen reduction activity of a gold electrode with the pyramidal structures was lower than those of the electrodes with the other nanostructures since the activity at the gold (111) surface is lower than that at the (100) and (110) surfaces.

Introduction

In the past couple of decades, there has been a burst of research activity on nanostructured metal particles, particularly noble metal nanoparticles with controlled size, morphology, and crystal orientation, because of their unique physical and chemical properties different from bulk metals.^{1,2} The synthesis of noble metal nanorods,³ nanowires,⁴ nanorings,⁵ nanobelts,⁶ and nanopolyhedrons,^{7,8} including nanocubes,⁹ nanoprisms,¹⁰ and nanoplates,¹¹ has been reported on the basis of their potential applications to materials and devices with a special electronic, optical, thermal, catalytic, or magnetic function.^{1,2,12–14} Among the noble metals, gold is of importance for its stability and unique optical properties.

In fabrication of such functional materials and devices, it is sometimes important to assemble the metal nanoparticles onto solid substrates. Charged polymers and other functional polymers have been employed to anchor the noble metal nanoparticles as a monolayer onto various substrates,^{15,16} including glasses, semiconductors, metals, and carbons. This self-assembly technique could also fabricate robust multilayers by layer-by-layer (LBL) assembly.^{17,18} Besides polymers, proteins¹⁹ and DNA²⁰ have also been exploited as anchoring agents. More recently, a templated self-assembly technique has been developed to fabricate three-dimensional nanoparticle arrays by using a nanoporous alumina template.²¹ In addition to these two-step methods, there have been reported methods for fabricating metal nanoparticle arrays on the basis of electron-beam lithography (EBL)²² or nanotemplating.^{23,24} However, these methods require expensive equipment or special templates.

Another useful method is electrochemical deposition.^{25–29} Various morphologies including rod-like²⁸ and dendritic^{29a} gold nanostructures have been obtained in a one-step process without templates, typically in the presence of an additive such as

Pb⁴⁺,^{25–28} cysteine,²⁹ or I[–].^{29b} However, those nanostructures were not necessarily well-defined. In this paper, we demonstrate one-step, inexpensive, nontemplated electrochemical fabrication of pyramidal, rod-like, and spherical gold nanostructures on a sputtered gold film. The structures are characterized by atomic force microscopy (AFM), visible spectroscopy, X-ray diffraction (XRD), and electrochemical methods. Their electrochemical activities for oxygen reduction are also examined.

Experimental Procedures

Chemicals and Materials. Hydrogen tetrachloroaurate(III) (HAuCl₄) trihydrate was purchased from Aldrich (St. Louis, MO) and used as supplied. Sodium hydroxide and perchloric acid were obtained from Wako Pure Chemical Industries, Ltd. (Osaka, Japan). The solution used in this work was freshly prepared Milli-Q water. ITO-coated glass plates with a square resistance of 10–20 Ω cm^{–2} were obtained from Asahi Glass (Japan).

Preparation of Gold Nanostructures. ITO-coated glass plates were thoroughly cleaned by sonication for 30 min in the following solvents successively: soapy water, water, neat acetone, and 1 M NaOH. Then, a gold film with a thickness of about 50 nm estimated by AFM was sputtered on the clean ITO glass plate. Pyramidal, rod-like, and spherical gold nanostructures were electrodeposited from aqueous solutions of 0.1 M HClO₄ containing 40, 4, and 40 mM HAuCl₄, respectively, at –0.08, –0.08, and –0.2 V versus Ag|AgCl, respectively, for 2 min.

Instruments and Measurements. An atomic force microscope SPA-300HV (Seiko Instruments Inc., Japan) was employed to record the images of the nanostructured gold surfaces. The XRD pattern was obtained by a D/max2550VB3+/PC X-ray diffractometer using Cu (40 kV, 100 mA). The visible reflectance spectra of the nanostructured surfaces were collected by a UV–vis spectrophotometer MCPD-3000 (Otsuka Electronics, Japan). A CHI 660 electrochemical work station (CH instruments, Austin, TX) was employed in all electrochemical

* Corresponding author. Tel: +86-21-65987075. Fax: +86-21-65982287. E-mail: yangtian@mail.tongji.edu.cn.

[†] Tongji University.

[‡] The University of Tokyo.

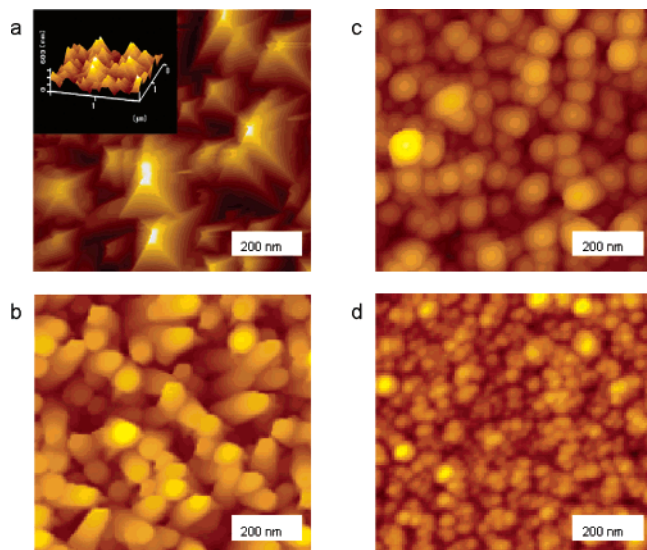


Figure 1. AFM images of the electrodeposited pyramidal (a), rod-like (b), and spherical (c) gold nanostructures and a sputtered gold surface (d). Similar images were obtained when different spots were scanned.

measurements, which were carried out with a conventional two-compartment three-electrode electrochemical cell. The reference electrode was a KCl-saturated Ag|AgCl electrode, while the auxiliary electrode was a platinum wire. The real surface area of gold nanostructures was determined by calculating the charge consumed during the formation of the surface oxide monolayer in H_2SO_4 solution.³⁰

Results and Discussion

Morphology of Gold Nanostructures. Gold nanostructures with various shapes were prepared by one-step and nontemplated electrochemical deposition under different experimental conditions. In the present work, we applied sufficiently negative potentials, -0.08 and -0.2 V versus Ag|AgCl, to the electrode, to obtain three-dimensional structures.

The morphology of the nanostructured gold films was characterized by AFM (Figure 1). As Figure 1a shows, deposition at -0.08 V versus Ag|AgCl in a 40 mM HAuCl_4 solution gave nanopyramidal structures. On the other hand, at a lower HAuCl_4 concentration (4 mM), rod-like nanostructures were obtained, as Figure 1b shows. At a more negative potential, -0.2 V, rather featureless spherical nanostructures formed in the 40 mM HAuCl_4 solution (Figure 1c). In the case of the nanopyramids, the edge length of the bottom was 50–200 nm, and the height was several hundreds of nanometers. The nanorods grew out to about 100 nm wide and up to 200–300 nm long, or more. The diameters of the nanospheres ranged from 70 to 100 nm. For comparison, an AFM image of the sputtered gold substrate is also shown in Figure 1d. Its spherical morphology with diameter of 25–50 nm is clearly different from the electrochemically deposited nanostructures, either in size or in shape.

Crystallographic Characterization. The crystalline orientation of the gold nanostructures was investigated by XRD. The diffraction peaks of the electrodeposited pyramidal, rod-like, and spherical gold nanostructures are shown in Figure 2a–c, respectively. The observed peaks corresponding to the (111), (200), (220), (311), and (222) facets demonstrate that the electrodeposited gold is composed of pure crystalline gold with the face-centered cubic (fcc) structure. The intensity ratios of the (200) peak to the (111) peak obtained for the pyramidal

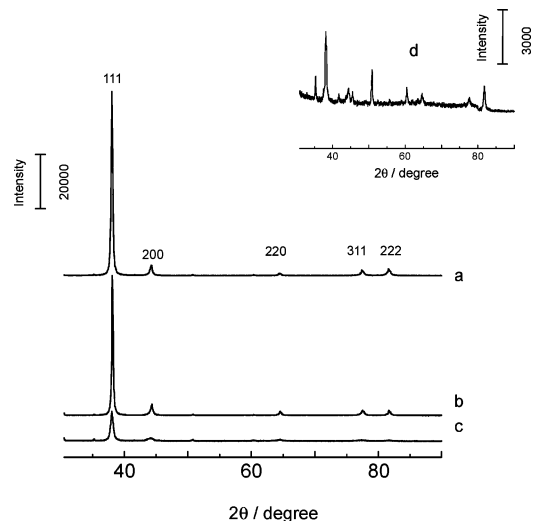


Figure 2. X-ray diffraction patterns of the electrodeposited pyramidal (a), rod-like (b), and spherical (c) gold nanostructures and a sputtered gold film (d).

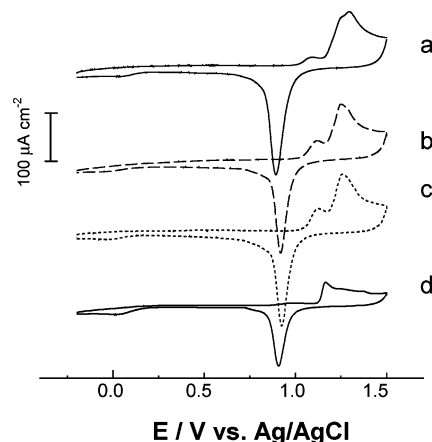


Figure 3. Cyclic voltammograms obtained at the electrodeposited pyramidal (a), rod-like (b), and spherical (c) gold nanostructure electrodes and a sputtered gold electrode (d) in 0.01 M aqueous H_2SO_4 . Potential scan rate: 50 mV s^{-1} .

(0.059), rod-like (0.078), and spherical (0.13) structures were much lower than that reported in the standard file (JCPDS, 0.33),¹¹ indicating that the gold nanostructures, nanopyramids in particular, were preferentially dominated by (111) facets. In contrast, the sputtered gold film exhibited a less prominent (111) peak (Figure 2d), in comparison with those for the electrochemically deposited nanostructures, indicating that the (100) and (110) facets constitute a considerable portion of the sputtered gold surface. Incidentally, the (222), (441), and (622) peaks of the ITO substrate are also seen in Figure 2d.

An electrochemical method was also employed for characterization. It is known that different gold facets show different cyclic voltammograms (CVs) in acidic solutions.³¹ Figure 3 depicts the CVs collected at the nanostructured gold electrodes in 0.01 M aqueous H_2SO_4 . It is noteworthy that the CV for the pyramidal nanostructure (Figure 3a), characterized by the oxidation peak at around +1.3 V versus Ag|AgCl, is characteristic of the gold (111) surface.³¹ In the case of the CVs for the rod-like and spherical nanostructures (Figure 3b,c, respectively), a small oxidation peak at around +1.1 V, which is indicative of the presence of the gold (100) and/or (110) facets,³¹ was observed, although there still was the large peak for the (111) surface. On the other hand, in the case of the CV for the sputtered gold, the peak for the (111) facets was much less

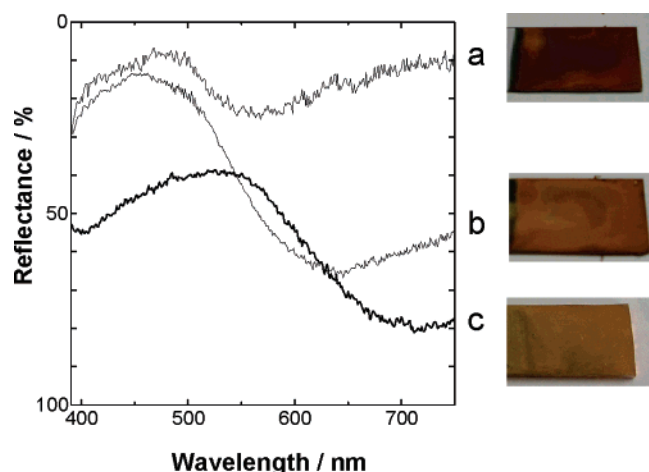


Figure 4. Visible reflectance spectra and the corresponding photographs of the electrodeposited pyramidal (a), rod-like (b), and spherical (c) gold nanostructures. Angle of incidence was 45° and that of detection was 0° .

significant. These results are qualitatively in agreement with the conclusions drawn from the XRD data.

Thus, it is reasonable to consider, on the basis of these results, that each nanopyramid is a gold single crystal with (111) facets. The nanopyramid can be recognized as a part of an octahedral gold nanocrystal, and octahedral gold crystals are normally enclosed by (111) facets. It is known that the (111) facet is the thermodynamically most stable among the possible facets of the fcc crystals. Therefore, it is rational that the crystal with the (111) facet is preferentially grown at a mild electrode potential, which enables relatively slow crystal growth, in a solution enriched with Au^{3+} .

Optical Properties. It is well-known that gold particles with nanometer-scale dimensions absorb light in the visible and/or near-infrared region due to localized plasmon resonance, which is light-induced collective oscillation of conduction electrons at the metal surface, and that the resonance wavelength depends on particle size, shape, and local dielectric environment.³² This is also the case for the nanostructured surfaces.³² Figure 4 demonstrates visible reflectance spectra and the corresponding photographs of the nanostructured gold surfaces. One broad extinction peak was observed at around 550 nm for the spherical structures (Figure 4c). For the rod-like structures, we can see an extinction peak at around 450 nm and an extinction increase from about 640 nm to the near-infrared region (Figure 4b). This is possibly due to splitting of a plasmon resonance band into longitudinal and transverse plasmon bands, corresponding to resonance along the long and short axes of the particle, respectively.^{3,33} More interestingly, the pyramidal structures exhibited extinction over the whole visible region (Figure 4a), consisting of at least two broad extinction bands. The highly anisotropic structure of the nanopyramids should be responsible for the multiple extinction bands, as is the case for gold nanoprisms¹⁰ and polyhedrons.^{7,8}

The roughness factors for the pyramidal, rod-like, and spherical nanostructures were estimated from AFM images to be 3.26 ± 0.05 , 2.43 ± 0.07 , and 1.21 ± 0.11 (average \pm standard error of three samples), respectively. Since the angles of incidence and detection were 45° and 0° , respectively, the reflectance should increase as the roughness increases for usual materials. In the present case, however, the reflectance decreased with the increasing roughness. The decrease is reasonably ascribed to the enhanced plasmon resonance and subsequently increased light absorption.

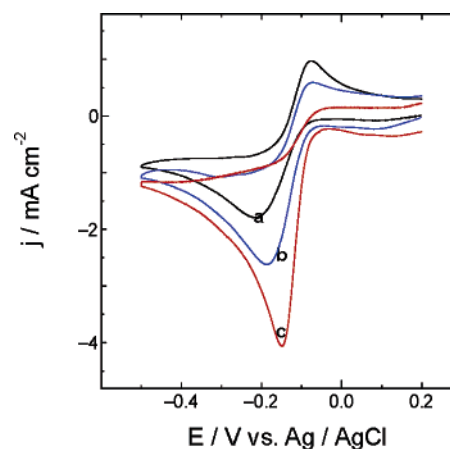
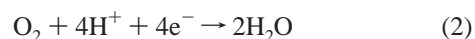
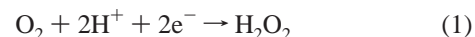


Figure 5. Cyclic voltammograms obtained at the electrodeposited pyramidal (a), rod-like (b), and spherical (c) gold nanostructure electrodes in O_2 -saturated 0.5 M aqueous KOH. Potential scan rate: 50 mV s^{-1} .

Electrocatalytic Activity for Oxygen Reduction. The electrocatalytic activity of the nanostructured gold films was examined toward oxygen reduction, which is a reaction of prime importance in view of its practical applications in chemical processing, energy conversion, and chemical sensing. Figure 5 represents CVs obtained at the pyramidal (a), rod-like (b), and spherical (c) gold nanostructures for the reduction of oxygen in 0.5 M KOH aqueous solution. The peak current increased and the peak potential shifted positively in the following order: nanopyramids < nanorods < nanospheres; namely, the more highly the surface is dominated by Au(111), the more reversible the oxygen reduction is. These results are reasonable because it has been reported that the oxygen reduction activity increases in the following order: $\text{Au}(111) < \text{Au}(110) < \text{Au}(100)$.^{30,34} Besides, Au(111) and Au(110) are known to be active toward two-electron reduction to hydrogen peroxide (eq 1), whereas Au(100) is active toward four-electron reduction to water (eq 2).³⁰



Therefore, the reaction selectivity can also be changed to some extent by controlling the nanostructures.

Conclusions

Pyramidal, rod-like, and spherical gold nanostructures were electrochemically prepared at different potentials and different HAuCl_4 concentrations. The nanopyramids were primarily dominated by (111) facets. The pyramidal nanostructures exhibited a unique plasmon-based color due to their anisotropic morphology and a low oxygen reduction activity owing to a lack of (100) and (110) facets, which are more active for the reaction than (111). The shape-controlled deposition of gold nanostructures would be useful in the development of gold films that are potentially applicable to electrocatalysis, surface-enhanced Raman scattering (SERS), surface plasmon sensors (SPR), and so on.

Acknowledgment. The authors are grateful to Dr. H. Notsu and K. Matsubara for their help with preliminary AFM experiments. This work was financially supported by the National Natural Science Foundation of China (NSFC 20643002).

and 20577035); the Shanghai Pujiang Program (06PJ14090); Tongji University; a Grant-in-Aid for Scientific Research on Priority Areas (Area 417, Research 14050028) from the Ministry of Education, Culture, Sports, Science and Technology of Japan; and a Grant-in-Aid for Scientific Research (17350064) from the Japan Society for the Promotion of Science (JSPS).

References and Notes

- (1) El-Sayed, M. A. *Acc. Chem. Res.* **2001**, *34*, 257–264.
- (2) Daniel, M. C.; Astruc, D. *Chem. Rev.* **2004**, *104*, 293–346.
- (3) Kim, F.; Song, J. H.; Yang, P. *J. Am. Chem. Soc.* **2002**, *124*, 14316–14317.
- (4) Hutchinson, Y. O.; Liu, Y.; Kiely, C.; Kiely, C. J.; Brust, M. *Adv. Mater.* **2001**, *13*, 1800–1803.
- (5) Sun, Y.; Xia, Y. *Adv. Mater.* **2003**, *15*, 695–699.
- (6) Zhang, J.; Du, J.; Han, B.; Liu, Z.; Jiang, T.; Zhang, Z. *Angew. Chem., Int. Ed.* **2006**, *45*, 1116–1119.
- (7) Kim, F.; Connor, S.; Song, H.; Kuykendall, T.; Yang, P. *Angew. Chem., Int. Ed.* **2004**, *43*, 3673–3677.
- (8) Chen, Y.; Gu, X.; Nie, C.; Jiang, Z.; Xie, Z.; Lin, C. *Chem. Commun.* **2005**, 4181–4183.
- (9) Sun, Y.; Xia, Y. *Science* **2002**, *298*, 2176–2179.
- (10) (a) Shankar, S. S.; Rai, A.; Ankamwar, B.; Singh, A.; Ahmad, A.; Sastry, M. *Nat. Mater.* **2004**, *3*, 482–488. (b) Millstone, J. E.; Park, S.; Shuford, K. L.; Qin, L.; Schatz, G. C.; Mirkin, C. A. *J. Am. Chem. Soc.* **2005**, *127*, 5312–5313.
- (11) Sun, X.; Dong, S.; Wang, E. *Angew. Chem., Int. Ed.* **2004**, *43*, 6360–6363.
- (12) Pendry, J. B. *Science* **1999**, *285*, 1687–1688.
- (13) (a) Tian, Y.; Tatsuma, T. *Chem. Commun.* **2004**, 1810–1811. (b) Tian, Y.; Tatsuma, T. *J. Am. Chem. Soc.* **2005**, *127*, 7632–7637.
- (14) (a) Ohko, Y.; Tatsuma, T.; Fujii, T.; Naoi, K.; Niwa, C.; Kubota, Y.; Fujishima, A. *Nat. Mater.* **2003**, *2*, 29–31. (b) Naoi, K.; Ohko, Y.; Tatsuma, T. *J. Am. Chem. Soc.* **2004**, *126*, 3664–3668.
- (15) Freeman, R. G. et al. *Science* **1995**, *267*, 1629–1632.
- (16) Doron, A.; Katz, E.; Willner, I. *Langmuir* **1995**, *11*, 1313–1317.
- (17) Liljeroth, P.; Quinn, B. M.; Ruiz, V.; Kontturi, D. J. *Chem. Commun.* **2003**, 1570–1571.
- (18) Jiang, C.; Markutsya, S.; Pikus, Y.; Tsukruk, V. V. *Nat. Mater.* **2004**, *3*, 721–728.
- (19) Qi, Z.; Honma, I.; Ichihara, M.; Zhou, H. *Adv. Funct. Mater.* **2006**, *16*, 377–386.
- (20) Mirkin, C. A.; Letsinger, R. L.; Mucic, R. C.; Storhoff, J. J. *Nature* **1996**, *382*, 607–608.
- (21) Lahav, M.; Sehayek, T.; Vaskevich, A.; Rubinstein, I. *Angew. Chem., Int. Ed.* **2003**, *42*, 5576–5579.
- (22) (a) Rechberger, W.; Hohenau, A.; Leitner, A.; Krenn, J. R.; Lamprecht, B.; Aussenegg, F. R. *Opt. Commun.* **2003**, *220*, 137–141. (b) Ueno, K.; Mizeikis, V.; Juodkasis, S.; Sasaki, K.; Misawa, H. *Opt. Lett.* **2005**, *30*, 2158–2160.
- (23) Foss, C. A., Jr.; Hornyak, G. L.; Stockert, J. A.; Martin, C. R. *J. Phys. Chem.* **1992**, *96*, 7497–7499.
- (24) van der Zande, B. M. I.; Böhmer, M. R.; Fokkink, L. G. J.; Scholtenberger, C. J. *Phys. Chem. B* **1997**, *101*, 852–854.
- (25) (a) Imamura, M.; Haruyama, T.; Kobatake, E.; Ikariyama, Y.; Aizawa, M. *Sens. Actuators, B* **1995**, *24*, 113–116. (b) Toyama, S.; Takei, O.; Tsugue, M.; Usami, R.; Horikoshi, K.; Kato, S. *Electrochem. Commun.* **2002**, *4*, 540–544.
- (26) van Noort, D.; Mandenius, C.-F. *Biosens. Bioelectron.* **2000**, *15*, 203–209.
- (27) Bonroy, K.; Friedt, J. M.; Frederix, F.; Laureyn, W.; Langerock, S.; Campitelli, A.; Sára, M.; Borghs, G.; Goddeeris, B.; Declerck, P. *Anal. Chem.* **2004**, *76*, 4299–4306.
- (28) Notsu, H.; Kubo, W.; Shitanda, I.; Tatsuma, T. *J. Mater. Chem.* **2005**, *15*, 1–6.
- (29) (a) Gao, E.; El-Deab, M. S.; Okajima, T.; Ohsaka, T. *J. Electrochem. Soc.* **2005**, *152*, 1226–1232. (b) El-Deab, M. S.; Sotomura, T.; Ohsaka, T. *J. Electrochem. Soc.* **2005**, *152*, 730–737.
- (30) El-Deab, M. S.; Arihara, K.; Ohsaka, T. *J. Electrochem. Soc.* **2004**, *151*, 213–218.
- (31) Hamelin, A. *J. Electroanal. Chem.* **1996**, *407*, 1–11.
- (32) Raether, H. *Surface plasmons on smooth and rough surfaces and on gratings*; Springer-Verlag: Berlin, 1988.
- (33) Murphy, C. J.; Sau, T. K.; Gole, A. M.; Orendorff, C. J.; Gao, J.; Gou, L.; Hunyadi, S. E.; Li, T. *J. Phys. Chem. B* **2005**, *109*, 13857–13870.
- (34) Schmidt, T. J.; Stamenkovic, V.; Arenz, M.; Markovic, N. M.; Ross, P. N., Jr. *Electrochim. Acta* **2002**, *47*, 3765–3776.